S1. Model description

S1.1 Aerosol

S1.1.1 Emissions

Anthropogenic (defined here as originating from industrial, energy, transportation, domestic and agriculture activity sectors) emissions are from the Lamarque et al. (2010) Intergovernmental Panel on Climate Change (IPCC) Fifth Assessment Report (AR5) emission dataset. Emissions of BC and organic carbon (OC) represent an update of Bond et al. (2007) and Junker and Liousse (2008). Emissions of SO_2 are an update of Smith et al. (2001; 2004).

The IPCC AR5 emission data set includes anthropogenic emissions for primary aerosol species and precursor gases: OC, BC, and SO_2. However, it does not provide injection heights and size distributions of primary emitted particles and precursor gases for which we have followed the AeroCom protocols (Dentener et al., 2006). We assumed that 2.5% (molar) of sulfur emissions are emitted directly as primary sulfate aerosols and the rest as SO_2 (Dentener et al., 2006). Sulfur from agriculture, domestic, transportation, waste, and shipping sectors is emitted at the surface while sulfur from energy and industry sectors is emitted at 100-300 m above the surface, and sulfur from forest fire and grass fire is emitted at higher elevations (0-6 km). Sulfate particles from agriculture, waste, and shipping (surface sources), and from energy, industry, forest fire and grass fire (elevated sources) are put in the accumulation mode, and those from domestic and transportation are put in the Aitken mode. We assumed that primary organic matter (POM) emissions are 1.4 time the primary OC emissions. POM and BC from forest fire and grass fire are emitted at 0-6 km, while those from other sources (domestic, energy,

industry, transportation, waste, and shipping) are emitted at the surface. Injection height profiles for forest fire and grass fire emissions are derived from the corresponding AeroCom profiles (Dentener et al., 2006), which give emissions in 6 altitude ranges (0-0.1, 0.1-0.5, 0.5-1, 1-2, 2-3, and 3-6 km). Emission rates (kg m^{-3} s^{-1}) are assumed uniform within each altitude range. Number emission fluxes for Aitken and accumulation mode particles are calculated from mass emission fluxes for sulfate, POM and BC based on AeroCom prescribed lognormal size distributions as summarized in Table S1.

The IPCC AR5 data set also does not provide emissions of natural aerosols and precursor gases: volcanic sulfur, DMS, NH_3, and biogenic volatile organic compounds (VOCs). Thus AeroCom emission fluxes, injection heights and size distributions for volcanic SO_2 and sulfate and the surface DMS flux are used. The emission flux for NH_3 is prescribed from the MOZART-4 data set (Emmons et al., 2010). Emission fluxes for isoprene, monoterprenes, toluene, big alkenes, and big alkanes, which are used to derive emissions of the semi-volatile organic species, are also prescribed from the MOZART-4 data set (Emmons et al., 2010). These emissions represent late 1990's conditions. For years prior to 2000, we use anthropogenic non-methane VOC (NMVOC) emissions from IPCC AR5 and scale the MOZART toluene, big alkene, and big alkane emissions by the ratio of year-of-interest NMVOC emissions to year 2000 NMVOC emissions.

The emission of sea salt aerosols from the ocean follows the parameterization by Märtensson et al. (2003) for aerosols with geometric diameter < 2.8 μm. The total number particle flux F_0 (m^{-2} s^{-1}) is described by

$$\frac{dF_0}{d\log D_p} = \Phi W = \left(A_k T_w + B_k\right) \cdot W \,, \qquad \text{(S1)}$$

where D_p is the particle diameter, T_w is the water temperature and A_k and B_k are coefficients dependent on the size interval. W is the white cap area:

$$W = 3.84 \times 10^{-4} \cdot U_{10}{}^{3.41}, \quad \text{(S2)}$$

where U_{10} is the wind speed at 10 m. For aerosols with a geometric diameter ≥ 2.8 μm, sea salt emissions follow the parameterization by Monahan et al. (1986):

$$\frac{dF_0}{d\log r} = 1.373 \cdot U_{10}{}^{3.41} r^{-3} \left(1 + 0.0057 r^{1.05}\right) \times 10^{1.19 e^{-B^2}}, \quad \text{(S3)}$$

where r is the radius of the aerosol at a relative humidity of 80% and B=(0.380-log$r$)/0.650. All sea salt emission fluxes in the model are calculated for a size interval of $d\log D_p$=0.1 and then summed up for each modal size range. The cut-off size ranges for sea salt emissions in MAM7 are 0.02-0.08 μm (Aitken), 0.08-0.3 μm (accumulation), 0.3-1.0 μm (fine sea salt), and 1.0-10 μm (coarse sea salt); for MAM3 the ranges are 0.02-0.08 μm (Aitken), 0.08-1.0 μm (accumulation), and 1.0-10 μm (coarse).

In regions of strong winds, dry un-vegetated soils generate soil particles small enough to be entrained into the atmosphere, which we refer as mineral dust particles. The generation of mineral dust particles is calculated based on the Dust Entrainment and Deposition Model (Zender et al., 2003), and the implementation in the Community Climate System Model has been described and compared to observations (Mahowald et al., 2006a; Mahowald et al., 2006b; Yoshioka et al., 2007). Here the only change in the source scheme from the previous studies is the increase in the threshold for leaf area index for the generation of dust from 0.1 to 0.3 m^2 m^{-2}, to be more consistent with observations of dust generation in more productive regions (Okin, 2008). The cut-off size range for dust emissions is 0.1-2.0 μm (fine dust) and 2.0-10 μm (coarse dust) for MAM7; and 0.1-1.0 μm (accumulation), and 1.0-10 μm (coarse) for MAM3. A lower

cut-off size at 1.0 μm is used between accumulation and coarse mode dust in MAM3 to limit the accumulation mode to submicron sizes.

S1.1.2 Chemistry

Simple gas-phase chemistry is included for sulfur species. This includes (1) DMS oxidation by OH and NO_3 to form SO_2; (2) SO_2 oxidation by OH to form H_2SO_4 (gas); (3) H_2O_2 production (HO_2+HO_2); and (4) H_2O_2 loss (H_2O_2 photolysis and H_2O_2+OH). The rate coefficients for these reactions are provided from the MOZART-4 model (Emmons et al., 2010). Oxidant concentrations (O_3, OH, HO_2, and NO_3) are temporally interpolated from monthly averages taken from simulations by a chemistry-climate model (CAM-Chem) (Lamarque et al., 2010).

SO_2 oxidation in bulk cloud water by H_2O_2 and O_3 is based on the MOZART treatment (Tie et al., 2001). The *p*H value in the bulk cloud water is calculated from the electroneutrality equation between the bulk cloud-borne SO_4 and NH_4 ion concentrations (summation over modes), and ion concentrations from the dissolution and dissociation of trace gases based on the Henry's law equilibrium. Irreversible uptake of H_2SO_4 (gas) to cloud droplets is also calculated (Seinfeld and Pandis, 1998). Sulfate produced from SO_2 aqueous oxidation and H_2SO_4 (gas) uptake is partitioned to increase the cloud-borne sulfate mixing ratio in each mode according to the ratio of the cloud-borne aerosol number among modes (i.e., the cloud droplet number associated with each aerosol mode) by assuming droplets associated with each mode have the same size. For MAM7, changes to aqueous NH_4 ion from dissolution of NH_3 are similarly partitioned among

modes. SO_2 and H_2O_2 mixing ratios are at the same time reduced due to aqueous phase consumption.

S1.1.3. SOA

The simplest treatment of SOA, which is used in many global models, is to assume fixed mass yields (i.e., percentages of precursor VOC amount that could form SOA) for anthropogenic and biogenic precursor VOC's, then directly emit this mass as primary aerosol particles. MAM adds one additional step of complexity by simulating a single lumped semi-volatile organics gas-phase species, which is referred to as SOAG in the model. Fixed mass yields of condensable organic vapor (i.e., the SOAG species) from five primary VOC categories of the MOZART-4 gas-phase chemical mechanism (Emmons et al., 2010) are assumed, as shown in Table S2. These yields have been increased by a factor of 1.5 during model tuning involving anthropogenic aerosol indirect forcing. Considering the large uncertainty with SOA formation, this factor is not unreasonable, and it brings our SOA and total organic aerosol sources close to some recent estimates (e.g., Heald et al., 2010; Spracklen et al., 2011). The resulting mass is emitted as the SOAG species with an emission of 103.3 Tg OM per year. MAM then calculates condensation/evaporation of the SOAG to/from several aerosol modes. The condensation/evaporation is treated dynamically, as described below. The equilibrium partial pressure of the SOAG gas, P_m^* over each aerosol mode *m* is expressed in terms of Raoult's Law as:

$$P_m^* = \left(\frac{A_m^{SOA}}{A_m^{SOA} + 0.1A_m^{POA}} \right) P^o \quad \text{(S4)}$$

,

where A_m^{SOA} is the SOA molar concentration in mode *m*, A_m^{POA} is the primary organic aerosol (POA) molar concentration in mode *m* (10% of which is assumed to be oxygenated), and P^0 is the mean saturation vapor pressure of the SOAG whose temperature dependence is expressed as:

$$P^0(T) = P^0(298K) \times \exp\left[\frac{-\Delta H_{vap}}{R}\left(\frac{1}{T} - \frac{1}{298}\right)\right], \quad \text{(S5)}$$

where P^0(298 K) is assumed at 1×10^{-10} atm and the mean enthalpy of vaporization ΔH_{vap} is assumed at 156 kJ mol^{-1}. *R* is the universal gas constant.

Treatment of this semi-volatile organics gas-phase species and explicit condensation/evaporation provides (1) a realistic method for calculating the distribution of SOA among different modes and (2) a minimal treatment of the temperature dependence of the gas/aerosol partitioning.

S1.1.4 Nucleation

New particle formation is calculated using parameterizations of binary H_2SO_4-H_2O homogeneous nucleation, ternary H_2SO_4-NH_3-H_2O homogeneous nucleation, and boundary layer nucleation. A binary parameterization (Vehkamaki et al., 2002) is used in the 3-mode version, which does not predict NH_3, while a ternary parameterization (Merikanto et al., 2007) is used in the 7-mode version. The boundary layer parameterization, which is applied in the planetary boundary layer (PBL) in both versions, uses the empirical first order (in H_2SO_4) nucleation rate from Sihto et al. (2006), with a first order rate coefficient of 1.0×10^{-6} s^{-1} as in Wang et al. (2009). The new particles are added to the Aitken mode, and we use the parameterization of Kerminen and

Kulmala (2002) to account for loss of the new particles by coagulation as they grow from critical cluster size to Aitken mode size.

S1.1.5. Condensation

Condensation of H_2SO_4 vapor, NH_3 (7 mode only), and the semi-volatile organics to various modes is treated dynamically, using standard mass transfer expressions (Seinfeld and Pandis, 1998) that are integrated over the size distribution of each mode (Binkowski and Shankar, 1995). An accommodation coefficient (i.e., the probability of sticking when a gas molecular encounters the surface of an aerosol particle) of 0.65 is used for H_2SO_4 (Poschl et al., 1998) and, currently, for the other species too. H_2SO_4 and NH_3 condensation are treated as irreversible. NH_3 uptake stops when the NH_4/SO_4 molar ratio of a mode reaches 2. SOA condensation is reversible, with the equilibrium vapor pressure over particles given by equation (S4).

In MAM7, condensation onto the primary carbon mode produces aging of the particles in this mode. Various treatments of the aging process have been used in other models (Cooke and Wilson, 1996; Wilson et al., 2001; Riemer et al., 2003; Liu et al., 2005). In MAM7, a criterion of 3 monolayers of sulfate is used to convert fresh POM/BC particles to the aged accumulation mode. Using this criterion and taking the diameter of particles in the mode, the mass of sulfate required to age all the particles in the primary carbon mode (by covering them all with 3 monolayers of sulfate), $M_{SO4,age\text{-}all}$, is computed. SOA is included in the aging process. The mass of SOA required to age all of the particles, $M_{SOA,age\text{-}all}$, is that which gives the same increase in volume-weighted hygroscopicity as $M_{SO4,age\text{-}all}$. If $M_{SO4,cond}$ (kg) of sulfate and $M_{SOA,cond}$ (kg) of SOA

condense on the aerosol particles in the primary carbon mode during a timestep, we assume that a fraction $f_{age} = (M_{SO4,cond} / M_{SO4,age\text{-}all} + M_{SOA,cond} / M_{SOA,age\text{-}all})$ has been aged. This fraction of the POM, BC, and number in the mode is transferred to the accumulation mode, along with the condensed soluble species.

The two continuous growth processes (condensation and aqueous chemistry) can result in Aitken mode particles growing to a size that is nominally within the accumulation mode size range. We thus transfer part of the Aitken mode number and mass (those particles on the upper tail of the distribution) to the accumulation mode after calculating continuous growth, following the approach of Easter et al. (2004).

S1.1.6. Coagulation

Intramodal and intermodal coagulation of the Aitken, accumulation, and primary carbon modes is treated. Coagulation involving modes with sizes larger than the accumulation mode (coarse modes, fine sea salt mode, and fine dust mode) is much slower (Binkowski and Roselle, 2003) and is neglected. Coagulation within each of these modes reduces number but leaves mass unchanged. For coagulation of Aitken with accumulation mode and of primary-carbon with accumulation mode, mass is transferred from Aitken or primary-carbon mode to the accumulation mode. For coagulation of Aitken with primary-carbon mode in MAM7, Aitken mass is first transferred to the primary-carbon mode. This ages some of the primary-carbon particles. An aging fraction is calculated as with condensation, then this Aitken mass and the aged fraction of the primary-carbon mass are both transferred to the accumulation mode. Coagulation

rates are calculated using the fast/approximate algorithms of the Community Multiscale Air Quality (CMAQ) model, version 4.6 (Binkowski and Roselle, 2003).

S1.1.7. Water Uptake

Water uptake is based on the equilibrium Köhler theory (Ghan and Zaveri, 2007) using the relative humidity and the volume-mean hygroscopicity for each mode to diagnose the wet volume-mean radius of the mode from the dry volume-mean radius. The hygroscopity of each component is listed in Table S3. The hygroscopicities here are equivalent to the κ parameters of Petters and Kreidenweis (2007). The hygroscopicities for sea salt, sulfate, ammonium, and SOA are from Petters and Kreidenweis (2007). The hygroscopicity for BC is set to be zero to represent its hydrophobic nature. Note that the measured hygroscopicity of dust varies widely, from 0.03 to 0.26 (Koehler et al., 2009), and a value of 0.068 is used in this study. The measured hygroscopicity of POM can vary from 0.0 for fossil fuel source to 0.06-0.30 for biomass burning source (Liu and Wang, 2010). We used a value of 0.1 for the hygroscopicity of POM in the standard CAM5, but investigated the sensitivity in section 5 to a smaller value of 0.0 to reflect the hydrophobic nature of POM from fossil fuel combustion.

S1.1.8 Subgrid Vertical Transport and Activation/Re-suspension

The vertical transport of interstitial aerosols and trace gases by deep convective clouds, using updraft and downdraft mass fluxes from the Zhang-McFarlane parameterization (Zhang and McFarlane, 1995), is described in Collins et al. (2004). Currently this vertical transport is calculated separately from wet removal, but a more

integrated treatment is planned. Cloud-borne aerosols associated with large-scale stratiform cloud are assumed to not interact with the convective clouds. Vertical transport by shallow convective clouds is treated similarly, using mass fluxes from the Park and Bretherton (2009) shallow convection parameterization.

Turbulent transport of the aerosol is given a special treatment with respect to other tracers. To strengthen the coupling between turbulent transport and aerosol activation in stratiform clouds, the implicit time integration scheme used for turbulent transport of heat, energy, and momentum is replaced by an explicit scheme for cloud droplets and aerosol. A sub-timestep calculation is performed for each column based on the minimum turbulent transport time in the column. Turbulent transport is integrated over the sub-time steps using a forward time integration scheme.

Aerosol activation converts particles from the interstitial attachment state to the cloud-borne state. In stratiform cloud, activation is treated consistently with droplet nucleation, so that the total number of particles activated and transferred to the cloud-borne state equals the number of droplets nucleated. Activation is parameterized in terms of updraft velocity and the properties of all of the aerosol modes (Abdul-Razzak and Ghan, 2000), with both mass and number transferred to the cloud-borne state. The updraft velocity is approximated by the square root of the turbulence kinetic energy, with a minimum value of 0.2 m s^{-1}. Activation is assumed to occur as updrafts carry air into the base of the cloud (Ghan et al., 1997) and as cloud fraction increases (Ovtchinnikov and Ghan, 2005). In addition, activation is assumed to occur as air is continuously cycled through clouds, assuming an in-cloud residence time for air parcels of three hours (Lelieveld and Crutzen, 1990, and references therein). For example, consider a model

time step of 30 minutes, so that 1/6 of the cloud volume is regenerated in a time step. We essentially dissipate and then reform 1/6 of the cloud in each time step. During dissipation, grid-cell mean cloud droplet number is reduced by 1/6, and 1/6 of the cloud-borne aerosols are re-suspended to the interstitial state. During regeneration, interstitial aerosols are activated in the "new" cloud, and cloud droplet number is increased accordingly. This regeneration has a small impact on shallow boundary layer clouds, but it noticeably increases droplet number in deeper free-tropospheric clouds where vertical mixing is slow. Cloud-borne aerosol particles (AP) are re-suspended as interstitial AP when droplets evaporate. This process is assumed to occur as droplets are transported below or above cloud and as clouds dissipate.

S1.1.9 Wet Removal

Aerosol wet removal is calculated using the CAM3.5 wet removal routine (Barth et al., 2000; Rasch et al., 2000) with modifications noted below. The routine treats in-cloud scavenging (the removal of cloud-borne AP) and below-cloud scavenging (the removal of interstitial AP by precipitation particles through impaction and Brownian diffusion).

For in-cloud scavenging, the precipitation production rates (kg kg^{-1} s^{-1}) and cloud water mixing ratios (kg kg^{-1}) for the stratiform and convective clouds are used to calculate first-order loss rates (s^{-1}) for cloud water. These cloud-water first-order loss rates are multiplied by "wet removal adjustment factors" (or tuning factors) to obtain aerosol first-order loss rates, which are applied to activated aerosols within the non-ice cloudy fractions of a grid cell (i.e., cloudy fractions that contain some cloud water). The stratiform in-cloud scavenging only affects the explicitly treated stratiform-cloud-borne

AP, and the adjustment factor of 1.0 is currently used. It does not affect the interstitial AP. In-cloud scavenging in ice clouds (i.e., clouds with no liquid water) is not treated.

For convective in-cloud scavenging of MAM aerosols, the cloud-borne aerosol mixing ratios within the convective clouds are needed. These are set to the product (lumped interstitial aerosol mixing ratio) × (convective-cloud activation fraction), and we again note that the model's lumped interstitial aerosol mixing ratios include the truly interstitial AP and the convective cloud-borne AP. The convective-cloud activation fractions are currently set to 0.0 for the primary carbon mode, 0.4 for the fine and coarse dust modes, and 0.8 for other modes. The lower values reflect lower hygroscopicity. These factors are applied to both number and mass species within each mode, with one exception. In MAM3, different activation fractions are applied to the dust and sea salt of the coarse mode (0.4 and 0.8 respectively), and a weighted average is applied to the coarse mode sulfate and number. A wet-removal adjustment factor of 0.5 is used for the convective in-cloud scavenging. The stratiform-cloud-borne AP reside in the stratiform clouds and are assumed to not interact with convective clouds.

For below-cloud scavenging of the interstitial aerosol, the first-order removal rate is equal to the product (scavenging coefficient) × (precipitation rate). The scavenging coefficient is calculated using the continuous collection equation (e.g., Equation 2 of Wang et al., 2011), in which the rate of collection of a single aerosol particle by a single precipitation particle is integrated over the aerosol and precipitation particle size distributions, at a precipitation rate of 1 mm h^{-1}. Collection efficiencies from Slinn (1984) and a Marshall-Palmer precipitation size distribution are assumed. The scavenging coefficient varies strongly with particle size, with lowest values for the accumulation

mode. The wet removal adjustment factor is currently 0.1. There is no below-cloud scavenging of stratiform-cloud-borne aerosol.

Aerosol that is scavenged at one altitude can be re-suspended at a lower altitude if precipitation evaporates. A fraction of the in-cloud scavenged aerosol is re-suspended, and the re-suspended fraction is equal to the fraction of precipitation that evaporates below cloud.

S1.1.10 Dry Deposition

Aerosol dry deposition velocities are calculated using the Zhang et al. (2001) parameterization with the CAM5 land-use and surface layer information. Gravitational settling velocities are calculated at all vertical layers above the surface following Seinfeld and Pandis (1998). Both velocities depend on particle wet size, so average values for aerosol mass and number are calculated for each mode. The velocities for cloud-borne aerosols are calculated based on droplet sizes. Aerosol mixing ratio changes and fluxes from dry deposition and sedimentation throughout a vertical column are then calculated using the CAM3 dust deposition/sedimentation routine (Zender et al., 2003).

S1.2 Clouds

In CAM5, two types of clouds may exist in each model grid-cell: 'stratus' and 'cumulus'. They are horizontally non-overlapped and have their own cloud fraction and condensate. Total cloud fraction is a sum of stratus and cumulus fractions because stratus is assumed to occupy non-cumulus area only. Both the stratus and cumulus are radiatively active.

Liquid and ice stratus fraction are treated separately. Liquid stratus fraction is obtained from the triangular probability density function (PDF) of total specific humidity using an externally specified half width of the distribution (Smith, 1990; Park et al., 2011). Ice stratus fraction is a quadratic function of relative humidity (RH) (Slingo, 1980; Rasch and Kristjansson, 1998), but with consideration of super-saturation over ice and grid-mean ice water content (IWC) (Gettelman et al., 2010). Total stratus fraction is the maximum of liquid and ice stratus fractions by assuming maximum overlap between liquid and ice.

Conversion of water vapor into stratus liquid water content (LWC) is computed using a prognostic saturation adjustment (Park et al., 2011) based on the assumptions that RH within liquid stratus is one and clear sky cannot hold cloud condensate. Thus, any water vapor exceeding saturation specific humidity over water within liquid stratus is condensed into cloud liquid, while any cloud liquid in the clear sky is evaporated until the clear sky is saturated. The sum of these two processes determines grid-mean net condensation rate. It is assumed that external advective forcing of conservative scalars (total specific humidity including water vapor and cloud condensate, q_t, and liquid potential temperature, θ_l) is uniform across the grid. In order to reduce inconsistency between in-stratus LWC and liquid stratus fraction, a pseudo condensation-evaporation is additionally applied until the in-cloud LWC is within a reasonable range (Park et al., 2011). In case of in-stratus IWC, we adjust the ice stratus fraction such that the resulting in-stratus IWC is within the specified lower and upper limits. These adjustment processes effectively remove both 'empty stratus' (i.e., non-zero cloud fraction but zero condensate) and 'dense-stratus' (i.e., zero cloud fraction but non-zero condensate). If net

evaporation occurs, cloud droplet number concentration decreases. This macrophysical treatment of liquid stratus is detailed in Park et al. (2011). The conversion of water vapor into stratus IWC is expressed in terms of ice particle surface area and supersaturation with respect to ice, as described by Liu et al. (2007) and Gettelman et al. (2010).

Stratus cloud microphysical processes are treated using the double-moment formulation of Morrison and Gettelman (2008) (MG08, thereafter) and Gettelman et al. (2008), which predicts number and mass mixing ratios of cloud droplets and ice crystals and diagnoses number and mass mixing ratios of rain and snow. The treatment of droplet nucleation in MG08 has been modified in CAM5 to be consistent with aerosol activation as described above. The treatment of ice nucleation in MG08 has also been modified in CAM5 following Liu et al. (2007), which includes homogeneous nucleation on sulfate competing with heterogeneous immersion on mineral dust in ice clouds (with temperature less than -37°C) (Liu and Penner, 2005). However, unlike Liu et al. (2007), immersion freezing on soot is not treated in CAM5. In the mixed-phase cloud regime (-37°C < T < 0°C), deposition/condensation/immersion nucleation is considered based on Meyers et al. (1992), and contact freezing of cloud droplets through Brownian coagulation with mineral dust is included (Young, 1974). Secondary ice production between -3° and -8°C (the Hallet-Mossop process) in mixed-phase clouds is included.

Cumulus consists of ‘shallow cumulus’ and ‘deep cumulus’, which are horizontally non-overlapped and have their own cloud fraction and condensate. Deep cumulus fraction is parameterized as an empirical logarithmic function of deep convective mass flux, while shallow cumulus fraction is computed using shallow convective updraft mass flux and vertical velocity. In-cumulus condensate is internally generated within each shallow and

deep convective scheme. The fraction of LWC among total convective condensate is a simple ramping function of temperature.

The shallow convection scheme is described in Park and Bretherton (2009). A single convective updraft plume with certain source air properties (q_t, θ_l and aerosol number and mass densities) is launched at the PBL top. The cloud base mass flux is determined from the mean turbulence kinetic energy (TKE) within the PBL and the inversion strength just above the PBL top (i.e., convective inhibition). Above the PBL, a portion of convective updraft mass is mixed with the same mass of environmental air. The amount of mass involved in the mixing is proportional to the updraft mass flux and the inverse of geometric height. The mixtures with positive buoyancy or with negative buoyancy with a vertical velocity strong enough to reach a certain level are entrained but the others are detrained. The entrainment and detrainment determine vertical profiles of convective updraft properties, which allow us to compute convective flux and the tendency of any conservative scalars.

At the cumulus top where an inversion layer exists, free air is entrained into the cumulus layer in proportion to the convective updraft mass flux. Within the PBL, the convective updraft flux is a simple linear function with zero value at the surface. The shallow convection scheme also computes the vertical velocity of the cumulus updraft. Core updraft fractional area is the updraft mass flux divided by the updraft vertical velocity and density. The saturated convective fractional area is set to be twice the core updraft fractional area. No convective downdrafts exist in the shallow convection scheme.

Shallow cumulus microphysics is very simple: if in-cumulus condensate is larger than a certain threshold, the excess is precipitated out. This means that no microphysical interaction exists between aerosol and convective condensate. Thus, aerosol indirect effect associated with cumulus is not simulated even though convective precipitation scavenges aerosols as mentioned above.

Deep convection is represented following a modified version of the Zhang-McFarlane parameterization (Zhang and McFarlane, 1995). The scheme represents an ensemble of buoyant plumes in bulk form and is closed on undilute Convectively Available Potential Energy (CAPE). Modifications to the scheme follow those used in Community Climate System Model version 3.5 (CCSM3.5) coupled climate simulations (Neale et al., 2008; Gent et al., 2009) with the inclusion of sub-grid convective momentum transports (Richter and Rasch, 2008) and the use of an entraining plume model to calculate a dilute CAPE used in the closure (Neale et al., 2008).

S1.3 Radiation

Longwave and shortwave radiative transfer are parameterized in CAM5 with the Rapid Radiative Transfer Model for GCMs (RRTMG), a broadband k-distribution radiation model developed for application to GCMs (Mlawer et al., 1997; Iacono et al., 2003; Iacono et al., 2008). Both RRTMG and the related single-column radiation model RRTM were developed in the context of continual comparison to the Line By Line Radiative Transfer Model (LBLRTM), which is an accurate, efficient and highly flexible line-by-line radiative transfer model that continues to be extensively validated with measured atmospheric radiance spectra from the sub-millimeter to the ultraviolet (Turner

et al., 2004; Clough et al., 2005). This realizes the objective of providing improved radiative transfer capability to GCMs that is directly traceable to measurements. Molecular absorbers in RRTMG include water vapor, carbon dioxide, ozone, methane, nitrous oxide, oxygen, nitrogen and the halocarbons in the longwave and water vapor, carbon dioxide, ozone, methane and oxygen in the shortwave. The water vapor continuum is based on CKD_v2.4, and molecular line parameters are based on HITRAN 2000 for water vapor and HITRAN 1996 for all other molecules. RRTMG uses sixteen spectral intervals to represent the longwave region, while the shortwave band is represented by fourteen spectral intervals. Absorption from aerosols and clouds are included in the longwave, and extinction from aerosols, clouds and Rayleigh scattering are treated in the shortwave.

While RRTMG shares the same basic physics and absorption coefficients as RRTM, it incorporates several modifications to improve computational efficiency, to update the code formatting for easier application to GCMs, and to represent sub-grid scale cloud variations. The complexity of representing fractional cloudiness and cloud overlap in the presence of multiple scattering is addressed in RRTMG with the use of McICA, the Monte-Carlo Independent Column Approximation (Pincus et al., 2003), which is a statistical technique for representing sub-grid scale cloud variability including cloud overlap. Although this method introduces random noise to the cloudy calculation of radiance, the result has been shown to be unbiased (Pincus et al., 2003). This approach provides the flexibility to represent the vertical correlation of the clouds (i.e. cloud overlap) in some detail by imposing an assumed relation (such as random or maximum-random) among the stochastic cloud arrays across the vertical dimension. The maximum-

random cloud overlap assumption, in which adjacent cloud layers in the vertical are presumed to overlap maximally and non-adjacent cloudy layers are assumed to overlap randomly, is used for this work.

Aerosol radiative effects are treated in RRTMG through the specification of their optical properties within each spectral interval. Aerosol optical properties are parameterized in terms of wet refractive index and wet surface mode radius according to Ghan and Zaveri (2007), except that volume mixing rule is used to calculate the volume-mean wet refractive index for mixtures of insoluble and soluble particles. We found little difference between the volume mixing treatment and the Maxwell-Garnett mixing rule. Refractive indices for most aerosol components are taken from OPAC (Hess et al., 1998), but for black carbon the value (1.95, 0.79i) from Bond and Bergstrom (2006) is used. Densities for each component are listed in Table S3.

Liquid cloud optics are implemented as a lookup table in terms of the λ (slope) and μ (shape) parameters of the gamma size distribution provided by the methods of Morrison and Gettelman (2008). The table elements are the wavelength and size-distribution averages of the extinction, single-scattering albedo, and asymmetry parameter resulting from Mie computations (Wiscombe, 1979) using the index of refraction of pure water. These elements are a function of selected slope and shape parameter values that cover the range of values generated by the stratiform microphysical code. The effect of in-cloud liquid water variability is not included in the generation of the lookup tables. The values of the slope and shape parameters for shallow and deep cumulus clouds are assumed to be the same as those for stratiform clouds if they exist in the same grid cell; otherwise

they are set to constant values corresponding to a shape parameter μ of 5.3 and an effective diameter of 25 μm.

CAM5 also uses a look-up table approach for the ice cloud optics. The mass-weighted extinction (volume extinction coefficient/ice water content) and the single scattering albedo, ω_o, in the ice optics look-up table were produced by the modified anomalous diffraction approximation (MADA), described by Mitchell (2000; 2002) and Mitchell et al. (2006). MADA calculates the extinction and absorption coefficients, β_{ext} and β_{abs}, and thus cloud optical depth and ω_o. The asymmetry parameter g is determined as a function of wavelength and ice particle size and shape as described by Gettelman et al. (2010). A shape recipe for ice crystals was assumed when calculating these optical properties, as well as for snow since the radiative effect of snow is also included (Gettelman et al., 2010)

Snow darkening from aerosol deposition is treated uniquely within the land and sea-ice components of CCSM. Deposited aerosols are apportioned into species conforming to the "bulk" aerosol scheme (Rasch et al., 2001) to which the Snow, Ice, and Aerosol Radiative (SNICAR) model was originally coupled (Flanner et al., 2007). Mapping of species from the modal aerosol scheme to bulk aerosols is listed in Table S4. In this mapping scheme, interstitial and in-cloud species are grouped together. Wet- and dry deposited-species are also treated together, once they have been received by the surface model components.

For each snowpack constituent, we assign mass-extinction coefficients ($m^2\,kg^{-1}$), single-scatter albedos, and scattering asymmetry parameters according to the spectral grid applied in each host model. SNICAR, embedded in the land model, applies five spectral

bands (0.3−0.7, 0.7−1.0, 1.0−1.2, 1.2−1.5, and 1.5−5.0 μm), whereas the sea-ice model utilizes a delta-Eddington scheme (Briegleb and Light, 2007) with three bands (0.3−0.7, 0.7−1.19, 1.19−5.0 μm). Hyper-spectral (470 band) optical properties are computed offline with Mie Theory, and weighted into these broad bands according to a surface-incident spectral flux distribution typical of mid-latitude winter (Flanner et al., 2007). Descriptions on the snow and sea-ice radiative transfer schemes, including tables with optical properties of all impurities and details of the weighting schemes applied to merge impurity and ice optical properties, are found, respectively, in Oleson et al. (2010) and Briegleb and Light (2007). We plan to implement future versions of the snow model that represent aerosols more consistently with the MAM3 and MAM7 schemes discussed here.

S1.4 Turbulence

The treatment of turbulence in CAM5 is described by Bretherton and Park (2009) and its performance is evaluated by Park and Bretherton (2009). The scheme expresses down-gradient diffusion of moist-conserved scalars and horizontal momentum within turbulent layers in terms of a TKE diagnosed from the local TKE production-transport-dissipation balance. The strong longwave radiative cooling at the cloud top is explicitly included in the TKE balance equation, which allows more realistic simulation of marine stratocumulus clouds. An explicit entrainment closure is used to diagnose an effective "entrainment diffusivity" at the edge of turbulent layers. All the scalars except aerosols and cloud liquid droplet number are diffused in an implicit way to reduce numerical instability due to the long model integration time step (1800 s) in CAM5.

S1.5 Resolved Transport

Transport of water and other trace species is calculated with the Lin-Rood finite volume dynamical core (Lin and Rood, 1996; Lin, 2004). Gent et al. (2009) describe the performance of this dynamical core at 0.5° resolution with CAM3.5 physics. Here we use the 1.9° latitude × 2.5° longitude resolution with 30 vertical layers in CAM5. There are five vertical layers below 900 hPa.

S2. Model evaluation

S2.1 Cloud Properties

In this subsection we compare model simulated cloud properties from MAM3 and MAM7 with available observations, which is important for the aerosol wet removal and aerosol indirect forcing. Figure S1 shows annual and zonal mean shortwave cloud forcing (SWCF), longwave cloud forcing (LWCF), liquid water path (LWP), and total cloud cover (CLDTOT) from MAM3 and MAM7 in comparison with available observations. The global annual mean values for these and other variables are given in Table S5. We can see that modeled SWCF is too strong in the tropics, but it is too weak in NH and SH high latitudes, in comparison with CERES data. Modeled LWCF is too low on the global scale compared with CERES data, as well as LWP with SSM/I data. Modeled total cloud cover is too low in the subtropics and mid-latitudes, but it is too high in the two polar regions, as compared to the ISCCP data. This too low LWP indicates too fast conversion of cloud water to precipitation and thus a too short lifetime of cloud water. This may partly explain the too large wet scavenging rates of aerosols (once they are inside the cloud water via droplet activation) and thus the too low burdens and short lifetimes of

aerosols (e.g., POM, SOA and BC). The too large cloud cover in the high latitudes of NH also contributes to the low concentrations of aerosol (e.g., BC) in the Arctic. Simulated cloud properties are very similar between MAM3 and MAM7 with a slightly higher column cloud droplet number concentration in MAM3 (Table S5), due to its larger sea salt concentrations. We note that the relative differences in CDNUMC are smaller than the differences in CCN at S=0.1% (Table S5).

Table S1. Size distributions of primary aerosol emissions.

Emission Source	Geometric standard deviation, σ_g	Number mode diameter, D_{gn} (μm)	D_{emit} (μm)[a]
BC/OM			
-Forest fire/grass fire	1.8	0.080	0.134
-Domestic/energy/industry/ transportation/waste/shipping	1.8[b]	0.080[b]	0.134[b]
SO_4			
-Forest fire/grass fire/waste/agriculture	1.8	0.080	0.134
-Energy/industry/shipping	-[c]	-[c]	0.261[c]
-Domestic/transportation	1.8	0.030	0.0504
-Continuous volcano, 50% in Aitken mode	1.8	0.030	0.0504
-Continuous volcano, 50% in accum. mode	1.8	0.080	0.134

a. D_{emit} is volume-mean diameter = $D_{gn} \times \exp(1.5 \times (\ln(\sigma_g))^2)$ used in number emissions as $E_{number} = E_{mass} / (\pi/6 \times \rho \ D_{emit}^3)$, and ρ is the aerosol particle density.
b. This D_{emit} value is in-between the lower value of 0.0504 μm used in Dentener et al. (2006) and higher value of 0.206 μm used in Liu et al. (2005).
c. Adapted from Stier et al. (2005) where 50% of the mass emissions from these sectors goes to the accumulation mode with D_{emit} = 0.207 μm, and 50% goes to the coarse mode with D_{emit} = 3.08 μm. We put all of these mass emissions in the accumulation mode, and D_{emit} = 0.261 μm gives the same number emissions as Stier et al. (2005). We note that Dentener et al. (2006) put all of these mass emissions in the coarse mode with D_{emit} = 2.06 μm.

Table S2. Assumed SOA yields.

Precursor species	Mass yield	Reference
Big Alkanes	5%	Lim and Ziemann (2005)
Big Alkenes	5%	assumed
Toluene	15%	Odum et al. (1997)
Isoprene	4%	Kroll et al. (2006)
Monoterpenes	25%	Ng et al. (2007)

Table S3. Hygroscopicity and density (kg m^{-3}) of aerosol components.

	Sea salt	Sulfate	Ammonium	SOA	POM	BC	Dust
Hygroscopicity	1.16	0.507	0.507	0.14	0.10	10^{-10}	0.068
Density	1900	1770	1770	1000	1000	1700	2600

Table S4. Mapping of absorbing species from the MAM3 and MAM7 to the bulk aerosol scheme.

Bulk Aerosol	MAM3	MAM7
Hydrophilic BC	Accumulation mode BC	Same as MAM3
Hydrophobic BC	-	Primary-carbon mode BC
Hydrophilic OC	Accumulation mode POM+SOA	Same as MAM3
Hydrophobic OC	-	Primary-carbon mode POM
Dust, bin 1 (finest)	Accumulation mode dust	Fine-dust mode dust
Dust, bin 2	-	-
Dust, bin 3	Coarse mode dust	Coarse-dust mode dust
Dust, bin 4 (coarsest)	-	-

Table S5. Global annual mean statistics from CAM5 with MAM3 and MAM7: shortwave (SWCF) and longwave (LWCF) cloud forcing, liquid water path (LWP), ice water path (IWP), total (CLDTOT), low (CLDLOW) and high (CLDHGH) cloud cover, column droplet number concentration (CDNUMC), column ice number concentration (CINUMC), and column CCN concentration at supersaturation of 0.1%.

Simulations	MAM3	MAM7	Observations
SWCF (W m^{-2})	-48.8	-48.9	-46 to -53[a]
LWCF (W m^{-2})	23.7	23.8	27-31[a]
LWP (g m^{-2})	41.0	40.7	50-87[b]
IWP (g m^{-2})	17.7	17.7	
CLDTOT (%)	62.9	63.0	65-75[c]
CLDLOW (%)	41.9	41.7	
CLDHGH (%)	38.0	38.4	21-33[d]
CDNUMC (10^{10} m^{-2})	1.27	1.19	
CINUMC (10^{10} m^{-2})	0.0092	0.0094	
Column CCN at S=0.1% (10^{10} m^{-2})	24.4	21.5	

a. SWCF, LWCF are from ERBE for the years 1985-1989 (Kiehl and Trenberth, 1997) and CERES for the years 2000-2005 (Loeb et al., 2009).
b. Liquid water path is derived from SSM/I (for the years 1987-1994, Ferraro et al., 1996; for August 1993 and January 1994, Weng and Grody, 1994; and for August 1987 and February 1988, Greenwald et al., 1993) and ISCCP for the year 1987 (Han et al., 1994). SSM/I data are restricted to oceans.
c. Total cloud fraction observations are obtained from ISCCP for the years 1983-2001 (Rossow and Schiffer, 1999), MODIS data for the years 2001-2004 (Platnick et al., 2003) and HIRS data for the years 1979-2001 (Wylie et al., 2005).
d. High cloud fraction observations are obtained from ISCCP data for the years 1983-2001 and HIRS for the years 1979-2001.

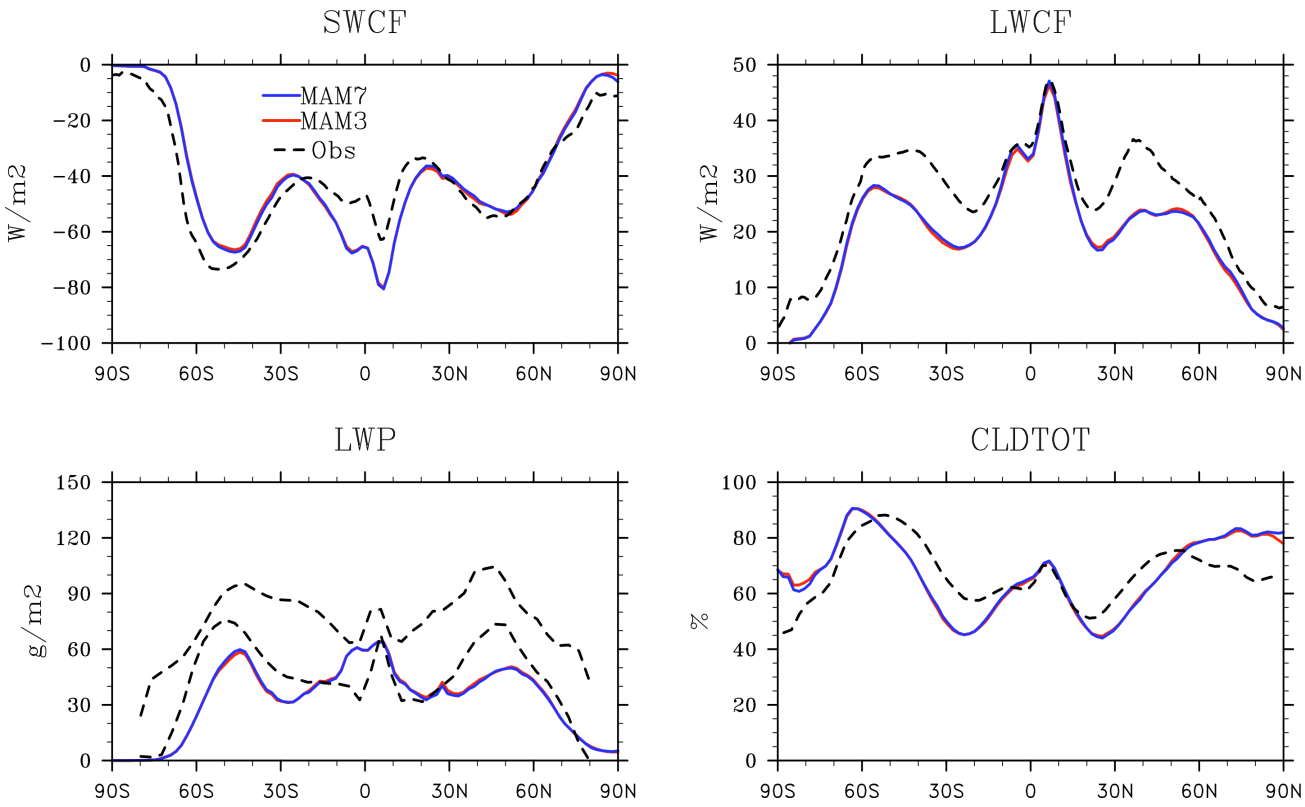

Figure S1. Annual and zonal mean shortwave cloud forcing (SWCF), longwave cloud forcing (LWCF), liquid water path (LWP), and total cloud cover (CLDTOT) from MAM3 and MAM7 in comparison with observations. Observed SWCF and LWCF are from CERES. Observed LWP is from SSM/I with two data sources: Weng and Grody (1994) (lower dashed line) and Greenwald et al. (1993) (upper dashed line). Observed CLDTOT is from ISCCP. LWP comparison is restricted to oceans.

References

Abdul-Razzak, H. and S. J. Ghan (2000). "A parameterization of aerosol activation 2. Multiple aerosol types." J. Geophysical Research-Atmospheres **105**(D5): 6837-6844.

Barth, M. C., P. J. Rasch, J. T. Kiehl, C. M. Benkovitz and S. E. Schwartz (2000). "Sulfur chemistry in the National Center for Atmospheric Research Community Climate Model: Description, evaluation, features, and sensitivity to aqueous chemistry." J. Geophysical Research-Atmospheres **105**(D1): 1387-1415.

Binkowski, F. S. and U. Shankar (1995). "The Regional Particulate Matter Model .1. Model description and preliminary results." J. Geophysical Research-Atmospheres **100**: 26191-26209.

Binkowski, F., and Roselle, S. (2003). "Models-3 community multiscale air quality (CMAQ) model aerosol component – 1. Model description". Journal Of Geophysical Research-Atmospheres, 108(D6), 4183. doi:10.1029/2001JD001409.

Bond, T. C. and R. W. Bergstrom (2006). "Light Absorption by Carbonaceous Particles: An Investigative Review." Aerosol Science and Technology **40**: 27–67.

Bond, T. C., G. Habib and R. W. Bergstrom (2006). "Limitations in the enhancement of visible light absorption due to mixing state." J. Geophysical Research-Atmospheres **111**(D20): D20211, DOI 10.1029/2006jd007315.

Bond, T. C., E. Bhardwaj, R. Dong, R. Jogani, S. K. Jung, C. Roden, D. G. Streets and N. M. Trautmann (2007). "Historical emissions of black and organic carbon aerosol from energy-related combustion, 1850-2000." Global Biogeochemical Cycles **21**(2): Gb2018, DOI 10.1029/2006gb002840.

Bretherton, C. S. and S. Park (2009). "A New Moist Turbulence Parameterization in the Community Atmosphere Model." J. Climate **22**(12): 3422-3448 DOI 10.1175/2008jcli2556.1.

Briegleb, B. P. and B. Light (2007). "A Delta-Eddington multiple scattering parameterization for solar radiation in the sea-ice component of the Community Climate System Model", National Center for Atmospheric Research Technical Note NCAR/TN-472+STR.

Clough, S. A., M. W. Shephard, E. Mlawer, J. S. Delamere, M. Iacono, K. Cady-Pereira, S. Boukabara and P. D. Brown (2005). "Atmospheric radiative transfer modeling: a summary of the AER codes." J. Quantitative Spectroscopy & Radiative Transfer **91**(2): 233-244 DOI 10.1016/J.Jqsrt.2004.05.058.

Collins, W. D., Rasch, P. J., Boville, B. A., Hack, J. J., McCaa, J. R., Williamson, D. L., Kiehl, J. T., Briegleb, B., Bitz, C., Lin, S.-J., Zhang, M.-H., Dai, Y. (2004). Description of the NCAR Community Atmosphere Model (CAM 3.0), National Center for Atmospheric Research Technical Note NCAR/TN–464+STR.

Cooke, W. F. and J. J. N. Wilson (1996). "A global black carbon aerosol model." J. Geophysical Research-Atmospheres **101**(D14): 19395-19409.

Dentener, F., et al. (2006). "Emissions of primary aerosol and precursor gases in the years 2000 and 1750 prescribed data-sets for AeroCom." Atmospheric Chemistry and Physics **6**: 4321-4344.

Easter, R. C., Ghan, S. J., Zhang, Y., Saylor, R. D., Chapman, E. G., Laulainen, N. S., Abdul-Razzak, H., Leung, L. R., Bian, X., and Zaveri, R. A. (2004). "MIRAGE:

Model description and evaluation of aerosols and trace gases." J. Geophysical Research-Atmospheres **109**(D20): DOI D20210,10.1029/2004jd004571.
Emmons, L. K., et al. (2010). "Description and evaluation of the Model for Ozone and Related chemical Tracers, version 4 (MOZART-4)." Geosci. Model Dev **3**: 43-67 DOI 10.5194/gmd-3-43-2010.
Ferraro, R. R., Weng, F. Z., Grody, N. C., and Basist, A. (1996). "An eightyear (1987-1994) time series of rainfall, clouds, water vapor, snow cover, and sea ice derived from SSM/I measurements", Bull. Amer. Meteor. Soc., 77, 891–905.
Flanner, M. G., C. S. Zender, J. T. Randerson and P. J. Rasch (2007). "Present-day climate forcing and response from black carbon in snow." J. Geophysical Research-Atmospheres **112**(D11): DOI 10.1029/2006jd008003.
Gent, P. R., Yeager, S. G., Neale, R. B., Levis, S., and Bailey, D. A. (2009). "Improvements in a half degree atmosphere/land version of the CCSM", Clim. Dynam., *79*, 25–58, doi:10.1007/s00382-009-0614-8.
Gettelman, A., H. Morrison and S. J. Ghan (2008). "A new two-moment bulk stratiform cloud microphysics scheme in the community atmosphere model, version 3 (CAM3). Part II: Single-colunm and global results." J. Climate **21**(15): 3660-3679 DOI 10.1175/2008jcli2116.1.
Gettelman, A., X. Liu, S. J. Ghan, H. Morrison, S. Park, A. J. Conley, S. A. Klein, J. Boyle, D. L. Mitchell, and J.-L. F. Li (2010), "Global simulations of ice nucleation and ice supersaturation with an improved cloud scheme in the Community Atmosphere Model." J. Geophysical Research-Atmospheres, 115, D18216, doi:10.1029/2009JD013797.
Ghan, S. J. and R. A. Zaveri (2007). "Parameterization of optical properties for hydrated internally mixed aerosol." J. Geophysical Research-Atmospheres **112**(D10): - DOI D10201, 10.1029/2006jd007927.
Ghan, S. J., L. R. Leung, R. C. Easter and K. Abdul-Razzak (1997). "Prediction of cloud droplet number in a general circulation model." J. Geophysical Research-Atmospheres **102**(D18): 21777-21794.
Greenwald, T. J., Stephens, G. L., Vonderhaar, T. H., and Jackson, D. L. (1993). "A physical retrieval of cloud liquid water over the global oceans using special sensor microwave imager (SSM/I) observations", J. Geophysical Research-Atmospheres, 98, 18471–18488.
Han, Q. Y., Rossow,W. B., and Lacis, A. A. (1994). "Near-Global survey of effective droplet radii in liquid water clouds using ISCCP data", J. Climate, 7, 465–497.
Heald, C. L., D. A. Ridley, S. M. Kreidenweis, and E. E. Drury (2010). "Satellite observations cap the atmospheric organic aerosol budget." Geophysical Research Letters, 37, doi:10.1029/2010GL045095.
Hess, M., P. Koepke and I. Schult (1998). "Optical properties of aerosols and clouds: The software package OPAC." Bulletin of the American Meteorological Society **79**(5): 831-844.
Iacono, M. J., J. S. Delamere, E. J. Mlawer and S. A. Clough (2003). "Evaluation of upper tropospheric water vapor in the NCAR Community Climate Model (CCM3) using modeled and observed HIRS radiances." J. Geophysical Research-Atmospheres **108**(D2): 4037, DOI 10.1029/2002jd002539.

Iacono, M. J., J. S. Delamere, E. J. Mlawer, M. W. Shephard, S. A. Clough and W. D. Collins (2008). "Radiative forcing by long-lived greenhouse gases: Calculations with the AER radiative transfer models." J. Geophysical Research-Atmospheres **113**(D13): D13103, DOI 10.1029/2008jd009944.

Junker, C. and C. Liousse (2008). "A global emission inventory of carbonaceous aerosol from historic records of fossil fuel and biofuel consumption for the period 1860-1997." Atmospheric Chemistry and Physics **8**(5): 1195-1207.

Kerminen, V. M. and M. Kulmala (2002). "Analytical formulae connecting the "real" and the "apparent" nucleation rate and the nuclei number concentration for atmospheric nucleation events." J. Aerosol Science **33**(4): 609-622 DOI Pii S0021-8502(01)00194-X.

Kiehl, J. T. and Trenberth, K. E. (1997). "Earth's annual global mean energy budget", Bull. Amer. Meteor. Soc., 78, 197–208.

Koehler, K. A., S. M. Kreidenweis, P. J. DeMott, M. D. Petters, A. J. Prenni and C. M. Carrico (2009). "Hygroscopicity and cloud droplet activation of mineral dust aerosol." Geophysical Research Letters **36**: L08805, DOI 10.1029/2009gl037348.

Kroll, J. H., N. L. Ng, S. M. Murphy, R. C. Flagan and J. H. Seinfeld (2006). "Secondary organic aerosol formation from isoprene photooxidation." Environmental Science & Technology **40**(6): 1869-1877 DOI 10.1021/Es0524301.

Lamarque, J. F., et al. (2010). "Historical (1850–2000) gridded anthropogenic and biomass burning emissions of reactive gases and aerosols: methodology and application." Atmospheric Chemistry and Physics **10**: 7017–7039.

Lelieveld, J., and P. J. Crutzen (1990). "Influences of cloud photochemical processes on tropospheric ozone." *Nature*, **343**, 227-233.

Lim, Y. B. and P. J. Ziemann (2005). "Products and mechanism of secondary organic aerosol formation from reactions of n-alkanes with OH radicals in the presence of NOx." Environmental Science & Technology **39**(23): 9229-9236 DOI 10.1021/Es051447g.

Lin, S. J. and R. B. Rood (1996). "Multidimensional flux-form semi-Lagrangian transport schemes." Monthly Weather Review **124**(9): 2046-2070.

Lin, S. J. (2004). "A "vertically Lagrangian" finite-volume dynamical core for global models." Monthly Weather Review **132**(10): 2293-2307.

Liu, X. H. and J. E. Penner (2005). "Ice nucleation parameterization for global models." Meteorologische Zeitschrift **14**(4): 499-514 DOI Doi 10.1127/0941-2948/2005/0059.

Liu, X. H., J. E. Penner and M. Herzog (2005). "Global modeling of aerosol dynamics: Model description, evaluation, and interactions between sulfate and nonsulfate aerosols." J. Geophysical Research-Atmospheres **110**(D18): D18206, Doi 10.1029/2004jd005674.

Liu, X. H., J. E. Penner, S. J. Ghan and M. Wang (2007). "Inclusion of ice microphysics in the NCAR community atmospheric model version 3 (CAM3)." J. Climate **20**(18): 4526-4547 DOI 10.1175/Jcli4264.1.

Liu, X., and J. Wang (2010). "How important is organic aerosol hygroscopicity to aerosol indirect forcing?" Environmental Research Letters, 5, 044010, doi: 10.1088/1748-9326/5/4/044010.

Loeb, N. G., Wielicki, B. A., Doelling, D. R., Smith, G. L., Keyes, D. F., Kato, S., Manalo-Smith, N., and Wong, T. (2009). "Toward Optimal Closure of the Earth's Top-of-Atmosphere Radiation Budget". J. Climate, 22, 748–766, doi:10.1175/2008jcli2637.1, 2009.

Mahowald, N., D. Muhs, S. Levis, P. Rasch, M. Yoshioka and C. Zender (2006a). "Change in atmospheric mineral aerosols in response to climate: last glacial period, pre-industrial, modern and doubled-carbon dioxide climates". J. Geophysical Research **111**: D10202, doi:10210.11029/12005JD006653.

Mahowald, N., M. Yoshioka, W. Collins, A. Conley, D. Fillmore and D. Coleman (2006b). "Climate response and radiative forcing from mineral aerosols during the last glacial maximum, pre-industrial and doubled-carbon dioxide climates." Geophysical Research Letters, **33**(L20705): doi:10.1029/2006GL026126.

Märtensson, E. M., E. D. Nilsson, G. de Leeuw, L. H. Cohen and H. C. Hansson (2003). "Laboratory simulations and parameterization of the primary marine aerosol production." J. Geophysical Research-Atmospheres **108**(D9): 4297, Doi 10.1029/2002jd002263.

Merikanto, J., I. Napari, H. Vehkamaki, T. Anttila and M. Kulmala (2007). "New parameterization of sulfuric acid-ammonia-water ternary nucleation rates at tropospheric conditions." J. Geophysical Research-Atmospheres **112**(D15): D15207, Doi 10.1029/2006jd007977.

Meyers, M. P., P. J. Demott and W. R. Cotton (1992). "New Primary Ice-Nucleation Parameterizations in an Explicit Cloud Model." J. Applied Meteorology **31**(7): 708-721.

Mitchell, D. L. (2000). "Parameterization of the Mie extinction and absorption coefficients for water clouds." J. the Atmospheric Sciences **57**(9): 1311-1326.

Mitchell, D. L. (2002). "Effective diameter in radiation transfer: General definition, applications, and limitations." J. the Atmospheric Sciences **59**(15): 2330-2346.

Mitchell, D. L., A. J. Baran, W. P. Arnott and C. Schmitt (2006). "Testing and comparing the modified anomalous diffraction approximation." J. the Atmospheric Sciences **63**(11): 2948-2962.

Mlawer, E. J., S. J. Taubman, P. D. Brown, M. J. Iacono and S. A. Clough (1997). "Radiative transfer for inhomogeneous atmospheres: RRTM, a validated correlated-k model for the longwave." J. Geophysical Research-Atmospheres **102**(D14): 16663-16682.

Morrison, H. and A. Gettelman (2008). "A new two-moment bulk stratiform cloud microphysics scheme in the community atmosphere model, version 3 (CAM3). Part I: Description and numerical tests." J. Climate **21**(15): 3642-3659 DOI 10.1175/2008jcli2105.1.

Neale, R. B., J. H. Richter and M. Jochum (2008). "The Impact of Convection on ENSO: From a Delayed Oscillator to a Series of Events." J. Climate **21**(22): 5904-5924 DOI 10.1175/2008jcli2244.1.

Ng, N. L., et al. (2007). "Effect of NOx level on secondary organic aerosol (SOA) formation from the photooxidation of terpenes." Atmospheric Chemistry and Physics **7**(19): 5159-5174.

Odum, J. R., T. P. W. Jungkamp, R. J. Griffin, H. J. L. Forstner, R. C. Flagan and J. H. Seinfeld (1997). "Aromatics, reformulated gasoline, and atmospheric organic aerosol formation." Environmental Science & Technology **31**(7): 1890-1897.

Okin, G. (2008). "A new model of wind erosion in the presence of vegetation." J. Geophysical Research-Earth Surface **113**(F02S10): doi:10.1029/2007JF000758.

Oleson, K.W., D.M. Lawrence, G.B. Bonan, M.G. Flanner, E. Kluzek, P.J. Lawrence, S. Levis, S.C. Swenson, P.E. Thornton, A. Dai, M. Decker, R. Dickinson, J. Feddema, C.L. Heald, F. Hoffman, J.-F. Lamarque, N. Mahowald, G.-Y. Niu, T. Qian, J. Randerson, S. Running, K. Sakaguchi, A. Slater, R. Stockli, A. Wang, Z.-L. Yang, Xi. Zeng, and Xu. Zeng, (2010). Technical Description of version 4.0 of the Community Land Model (CLM). NCAR Technical Note NCAR/TN-478+STR, National Center for Atmospheric Research, Boulder, CO, 257 pp.

Ovtchinnikov, M. and S. J. Ghan (2005). "Parallel simulations of aerosol influence on clouds using cloud-resolving and single-column models." J. Geophysical Research-Atmospheres **110**(D15): - DOI D15s10, 10.1029/2004jd005088.

Park, S., C. Bretherton and P. J. Rasch (2011). The global cloud simulations in the community atmosphere model CAM5, in preparation.

Park, S. and C. S. Bretherton (2009). "The University of Washington Shallow Convection and Moist Turbulence Schemes and Their Impact on Climate Simulations with the Community Atmosphere Model." J. Climate **22**(12): 3449-3469 DOI 10.1175/2008jcli2557.1.

Petters, M. D. and S. M. Kreidenweis (2007). "A single parameter representation of hygroscopic growth and cloud condensation nucleus activity." Atmospheric Chemistry and Physics **7**(8): 1961-1971.

Pincus, R., H. W. Barker and J. J. Morcrette (2003). "A fast, flexible, approximate technique for computing radiative transfer in inhomogeneous cloud fields." J. Geophysical Research-Atmospheres **108**(D13): 4376, DOI 10.1029/2002jd003322.

Platnick, S., King, M. D., Ackerman, S. A., Menzel, W. P., Baum, B. A., Riedi, J. C., and Frey, R. A. (2003). "The MODIS cloud products: Algorithms and examples from Terra", IEEE Trans. Geosci. Remote Sens., 41, 459–473.

Poschl, U., M. Canagaratna, J. T. Jayne, L. T. Molina, D. R. Worsnop, C. E. Kolb and M. J. Molina (1998). "Mass accommodation coefficient of H2SO4 vapor on aqueous sulfuric acid surfaces and gaseous diffusion coefficient of H2SO4 in N-2/H2O." J. Physical Chemistry A **102**(49): 10082-10089.

Rasch, P. J. and J. E. Kristjansson (1998). "A comparison of the CCM3 model climate using diagnosed and predicted condensate parameterizations." J. Climate **11**(7): 1587-1614.

Rasch, P. J., M. C. Barth, J. T. Kiehl, S. E. Schwartz and C. M. Benkovitz (2000). "A description of the global sulfur cycle and its controlling processes in the National Center for Atmospheric Research Community Climate Model, Version 3." J. Geophysical Research-Atmospheres **105**(D1): 1367-1385.

Rasch, P. J., W. D. Collins and B. E. Eaton (2001). "Understanding the Indian Ocean Experiment (INDOEX) aerosol distributions with an aerosol assimilation." J. Geophysical Research-Atmospheres **106**(D7): 7337-7355.

Richter, J. H. and P. J. Rasch (2008). "Effects of convective momentum transport on the atmospheric circulation in the community atmosphere model, version 3." J. Climate **21**(7): 1487-1499 DOI 10.1175/2007jcli1789.1.

Riemer, N., H. Vogel, B. Vogel and F. Fiedler (2003). "Modeling aerosols on the mesoscale-gamma: Treatment of soot aerosol and its radiative effects." J. Geophysical Research-Atmospheres **108**(D19): 4601, DOI 10.1029/2003jd003448.

Rossow, W. B. and Schiffer, R. A. (1999). "Advances in understanding clouds from ISCCP", Bull. Amer. Meteor. Soc., 80, 2261–2287.

Seinfeld, J. H. and S. N. Pandis (1998). Atmospheric Chemistry and Physics: From Air Pollution to Climate Change. Hoboken, N. J, John Wiley.

Sihto, S. L., et al. (2006). "Atmospheric sulphuric acid and aerosol formation: implications from atmospheric measurements for nucleation and early growth mechanisms." Atmospheric Chemistry and Physics **6**: 4079-4091.

Slingo, J. M. (1980). "A Cloud Parametrization Scheme Derived from Gate Data for Use with a Numerical-Model." Quarterly J. Royal Meteorological Society **106**(450): 747-770.

Slinn, W. G. N. (1984). Precipitation scavenging, in *Atmospheric Science and Power Production,* edited by D. Randerson, pp. 472-477, U. S. Dept. of Energy, Washington D. C.

Smith, R. N. B. (1990). "A scheme for predicting layer clouds and their water content in a general circulation model." Quarterly J. Royal Meteorological Society **116**: 435-460.

Smith, S. J., R. Andres, E. Conception and J. Lurz (2004). Historical Sulfur Dioxide Emissions 1850–2000: Methods and Results, Pacific Northwest National Laboratory, Joint Global Change Research Institute.

Smith, S. J., H. Pitcher and T. M. L. Wigley (2001). "Global and regional anthropogenic sulfur dioxide emissions." Global and Planetary Change **29**(1-2): 99-119.

Spracklen, D. V., et al. (2011). "Aerosol mass spectrometer constraint on the global secondary organic aerosol budget." Atmospheric Chemistry and Physics **11**(23), 12109-12136.

Stier, P., et al. (2005). "The aerosol-climate model ECHAM5-HAM." Atmospheric Chemistry and Physics **5**: 1125-1156.

Tie, X., G. Brasseur, L. Emmons, L. Horowitz and D. Kinnison (2001). "Effects of aerosols on tropospheric oxidants: A global model study." J. Geophysical Research-Atmospheres **106**(D19): 22931-22964.

Turner, D. D., Tobin, D. C., Clough, S. A., Brown, P. D., Ellingson, R. G., Mlawer, E. J., Knuteson, R. O., Revercomb, H. E., Shippert, T. R., Smith, W. L., and Shephard, M. W. (2004). "The QME AERI LBLRTM: A closure experiment for downwelling high spectral resolution infrared radiance." J. the Atmospheric Sciences **61**(22): 2657-2675.

Vehkamaki, H., M. Kulmala, I. Napari, K. E. J. Lehtinen, T. T., N. Noppel and A. Laaksonen (2002). "An improved parameterization for sulfuric acid-water nucleation rates for tropospheric and stratospheric conditions." J. Geophysical Research-Atmospheres **107**: 4622 DOI 10.1029/2002jd002184.

Wang, X., L. Zhang, and M. D. Moran (2011). "Uncertainty assessment of current size-resolved parameterizations for below-cloud particle scavenging by rain." Atmospheric Chemistry and Physics, **10**, 5685-5705. doi:10.5194/acp-10-5685-2010.

Weng, F. Z. and Grody, N. C. (1994). "Retrieval of cloud liquid water using the Special Sensor Microwave Imager (SSM/I)", J. Geophysical Research-Atmospheres, 99, 25535–25551.

Wilson, J., C. Cuvelier and F. Raes (2001). "A modeling study of global mixed aerosol fields." J. Geophysical Research-Atmospheres **106**(D24): 34,081–034,108.

Wiscombe, W. J. (1979). Mie scattering calculations: Advances in technique and fast, vector-speed computer codes, National Center for Atmospheric Research Tech. Note TN-140+STR**:** 62 pp.

Wylie, D., Jackson, D. L., Menzel, W. P., and Bates, J. J. (2005). "Trends in global cloud cover in two decades of HIRS observations", J. Climate, 18, 3021–3031.

Yoshioka, M., N. Mahowald, A. Conley, W. Collins, D. Fillmore and D. Coleman (2007). "Impact of desert dust radiative forcing on Sahel precipitation: relative importance of dust compared to sea surface temperature variations, vegetation changes and greenhouse gas warming." J. Climate **20**(DOI:10.1175/JCLI4056.1): 1445-1467.

Young, K. C., (1974). "The role of contact nucleation in ice phase initiation in clouds." J. Atmos. Sci., 31, 768–776.

Zender, C., H. Bian and D. Newman (2003). "Mineral Dust Entrainment and Deposition (DEAD) model: Description and 1990s dust climatology." J. Geophysical Research **108**(D14): 4416, doi:4410.1029/2002JD002775.

Zhang, G. J. and N. A. McFarlane (1995). "Sensitivity of Climate Simulations to the Parameterization of Cumulus Convection in the Canadian Climate Center General-Circulation Model." Atmosphere-Ocean **33**(3): 407-446.

Zhang, L. M., S. L. Gong, J. Padro and L. Barrie (2001). "A size-segregated particle dry deposition scheme for an atmospheric aerosol module." Atmospheric Environment **35**(3): 549-560.